

# Resonance parameters of the first $1/2^+$ state in ${}^9\text{Be}$ and astrophysical implications

O. Burda and P. von Neumann-Cosel\*

*Institut für Kernphysik, Technische Universität Darmstadt, D-64289 Darmstadt, Germany*

A. Richter

*Institut für Kernphysik, Technische Universität Darmstadt, D-64289 Darmstadt, Germany and  
ECT\*, Villa Tambosi, I-38123 Villazzano (Trento), Italy*

C. Forssén

*Fundamental Physics, Chalmers University of Technology, SE-412 96 Göteborg, Sweden*

B. A. Brown

*Department of Physics and Astronomy, and National Superconducting Cyclotron Laboratory,  
Michigan State University, East Lansing, Michigan 48824-1321, USA*

(Dated: August 9, 2018)

Spectra of the  ${}^9\text{Be}(e, e')$  reaction have been measured at the S-DALINAC at an electron energy  $E_0 = 73$  MeV and scattering angles of  $93^\circ$  and  $141^\circ$  with high energy resolution up to excitation energies  $E_x = 8$  MeV. The astrophysically relevant resonance parameters of the first excited  $1/2^+$  state of  ${}^9\text{Be}$  have been extracted in a one-level approximation of  $R$ -matrix theory resulting in a resonance energy  $E_R = 1.748(6)$  MeV and width  $\Gamma_R = 274(8)$  keV in good agreement with the latest  ${}^9\text{Be}(\gamma, n)$  experiment but with considerably improved uncertainties. However, the reduced  $B(E1)$  transition strength deduced from an extrapolation of the  $(e, e')$  data to the photon point is a factor of two smaller. Implications of the new results for a possible production of  ${}^{12}\text{C}$  in neutron-rich astrophysical scenarios are discussed.

PACS numbers: 25.30.Dh, 27.20.+n, 26.30.Ef, 26.20.Kn

## I. INTRODUCTION

The nucleus  ${}^9\text{Be}$  is a loosely-bound system formed by two  $\alpha$  particles and a neutron where none of any two constituents alone can form a bound system. It has the lowest neutron threshold  $S_n = 1.6654$  MeV of all stable nuclei. Already the first excited state lies some tens of keV above the neutron threshold and thus all excited states are unstable with respect to neutron decay.

The properties of the first excited state are of particular interest because they determine the importance of  ${}^9\text{Be}$  production for the synthesis of  ${}^{12}\text{C}$  seed material triggering the  $r$  process in type II supernovae [1–4]. In stellar burning the triple  $\alpha$  process dominates the production of  ${}^{12}\text{C}$ , where at sufficiently high temperatures a small equilibrium amount of the short-lived  ${}^8\text{Be}$  is formed, which can capture the third  $\alpha$  particle and form  ${}^{12}\text{C}$ . But in explosive nucleosynthesis, such as a core-collapse supernova, the reaction path  ${}^8\text{Be}(n, \gamma){}^9\text{Be}(\alpha, n){}^{12}\text{C}$  may provide an alternative route for building up heavy elements.

A direct measurement of the cross sections of the  ${}^8\text{Be}(n, \gamma){}^9\text{Be}$  reaction is impossible because of the short life time of about  $10^{-16}$  s of the  ${}^8\text{Be}$  ground state (g.s.) but they can be deduced from photodisintegration cross sections on  ${}^9\text{Be}$  using the principle of detailed balance. At low energies, the photodisintegration cross section is

dominated by the properties of the  $1/2^+$  resonance just above the  ${}^8\text{Be} + n$  threshold in  ${}^9\text{Be}$ . The description of this unbound level, viz. its resonance energy and width is a long-standing problem. Due to its closeness to the neutron threshold the resonance has a strongly asymmetric line shape.

Several experiments have investigated the  ${}^9\text{Be}(\gamma, n)$  reaction, either with real photons from bremsstrahlung or from laser-induced Compton backscattering, and with virtual photons from electron scattering (see Ref. [5] for a discussion and references). But despite the sizable body of data there still exist considerable uncertainties of the resonance parameters. Utsunomiya et al. [6] measured the photoneutron cross section for  ${}^9\text{Be}$  with real photons in the whole energy range of astrophysical relevance. The deduced resonance parameters for the  $1/2^+$  state are shown in Tab. I in comparison with results from earlier electron scattering experiments [7, 8]. Another recent result from  ${}^9\text{Li}$   $\beta$  decay ( $E_R = 1.689(10)$  MeV,  $\Gamma_R = 224(7)$  keV) is quoted by Ref. [9] but it is not clear whether these values refer to the true resonance parameters or the peak and full width at half maximum (FWHM). Furthermore, the results have been questioned by Barker and Fynbo [10]. Table I provides a summary of resonance parameters deduced from the various experiments.

Obviously there are significant differences between the results obtained from photonuclear and electron scattering experiments. The discrepancy in the  $B(E1)$  transition strength amounts to a factor of about two when com-

---

\*Electronic address: vnc@ikp.tu-darmstadt.de

TABLE I: Summary of resonance parameters and reduced transition probability of the  $1/2^+$  state in  ${}^9\text{Be}$  deduced from different experiments. Reference [11] contains a reanalysis of the data of [7].

Reaction	Ref.	$E_R$ (MeV)	$\Gamma_R$ (keV)	$B(E1)\uparrow$ ( $e^2\text{fm}^2$ )
( $e,e'$ )	[7]	1.684(7)	217(10)	0.027(2)
( $e,e'$ )	[8]	1.68(15)	200(20)	0.034(3)
( $\gamma,n$ )	[6]	1.750(10)	283(42)	0.0535(35)
( $e,e'$ )	[11]	1.732	270	0.0685
$\beta$ -decay	[9]	1.689(10)	224(7)	-
( $e,e'$ )	present	1.748(6)	274(8)	0.027(2)

paring with the results of ( $e,e'$ ) measurements [7, 12] at low momentum transfers  $q$ , while it is reduced by  $\sim 30\%$  in an ( $e,e'$ ) experiment [8] at larger  $q$ . The reason for these discrepancies between the strengths deduced from the real photon and virtual photon experiments is unknown. Furthermore, Barker [11] reanalyzed the ( $e,e'$ ) data of KÜchler et al. [7] and extracted resonance parameters which differ considerably from those quoted in the original paper (see Tab. I).

In order to resolve these discrepancies, high-resolution measurements of the  ${}^9\text{Be}(e,e')$  reaction were performed at the S-DALINAC and new resonance parameters for the  $1/2^+$  state are extracted. Furthermore, an independent reanalysis of the electron scattering data of KÜchler et al. [7] was performed. Finally, the temperature dependence of the  ${}^8\text{Be}(n,\gamma){}^9\text{Be}$  reaction rate including the new results is derived and compared to that of the NACRE compilation [13] serving as standard for most network calculations.

## II. EXPERIMENT

The  ${}^9\text{Be}(e,e')$  experiment was carried out at the high-resolution  $169^\circ$  magnetic spectrometer of the Superconducting Darmstadt Electron Linear Accelerator (S-DALINAC). Data were taken at an incident electron beam energy  $E_0 = 73$  MeV and scattering angles  $\Theta_{\text{Lab}} = 93^\circ$  and  $141^\circ$  with typical beam currents of  $2 \mu\text{A}$ . For the measurements a self-supporting  ${}^9\text{Be}$  target with an areal density of  $5.55 \text{ mg/cm}^2$  was used. The properties of the spectrometer are described in Ref. [14]. A new focal plane detector system based on silicon microstrip detectors was recently implemented [15]. In dispersion-matching mode an energy resolution  $\Delta E \simeq 30$  keV (full width at half maximum, FWHM) was achieved in the measurements.

Figure 1 presents the spectra of the  ${}^9\text{Be}(e,e')$  reaction measured up to an excitation energy of about 8 MeV. There is only one narrow peak visible in the spectra which corresponds to the excitation of the  $J^\pi = 5/2^-$  state at  $E_x = 2.429$  MeV. The tiny peak at about 4.2 MeV in both spectra correspond to the first excited state in  ${}^{12}\text{C}$

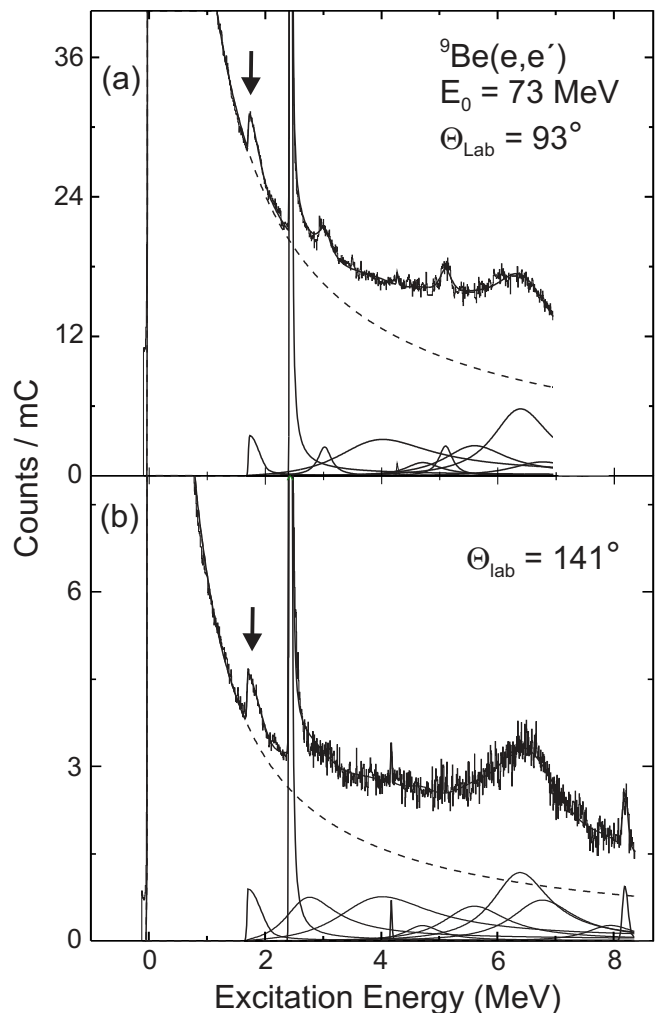


FIG. 1: Spectra of the  ${}^9\text{Be}(e,e')$  reaction at  $E_0 = 73$  MeV and  $\Theta_{\text{lab}} = 93^\circ$  (top) and  $141^\circ$  (bottom) and their decomposition. Solid lines: Fits to experimentally known resonances. Dashed lines: Radiative tail from elastic scattering. The arrows indicate the transition to the first excited state, whose asymmetric line shape is clearly visible.

(the deviation between the observed and the true excitation energy  $E_x = 4.439$  MeV stems from the difference of the recoil correction for nuclei with mass  $A = 9$  and  $12$ , respectively). The bumps around 5.1 MeV in the top spectrum and around 8.1 MeV in the bottom spectrum are due to elastic scattering on hydrogen. The broad bump between 6 and 7 MeV results from the overlap of resonances at  $E_x = 6.38$  MeV ( $J^\pi = 7/2^-$ ) and  $E_x = 6.76$  MeV ( $J^\pi = 9/2^+$ ) in  ${}^9\text{Be}$  [8]. The asymmetric line shape of the  $1/2^+$  state at  $E_x \approx 1.7$  MeV (marked by arrows Fig. 1) in is already clearly visible in the raw spectra.

In the decomposition of the spectra, the line shape of the narrow state was described by the function given in Ref. [16], whose parameters were determined by a fit to the elastic line. This also determines the background from the radiative tail of the elastic line in the region

of interest indicated by the dashed lines in Fig. 1. The line shapes of the broad resonances were assumed to correspond to an energy-dependent Breit-Wigner function discussed below. The energies and widths of the resonances (taken from the latest compilation [5]) were kept fixed during the fit except for the parameters of the first excited state. Finally, the  $1/2^+$  resonance was treated in a one-level  $R$ -matrix formalism explained in the next section.

### III. ANALYSIS

Since the state of interest lies above the neutron threshold, we first discuss an extraction of the relevant parameters as if it was excited in a  $(\gamma, n)$  reaction. In Sec. III B, the relation to the  $(e, e')$  data is explained. Finally, Sec. III C describes the extraction of the resonance parameters.

#### A. One-level $R$ -matrix approximation

The contribution to the  $(\gamma, n)$  cross section from an isolated level of spin  $J$  located near threshold in the one-level approximation of  $R$ -matrix theory [17] is given by

$$\sigma_{\gamma, n}(E_\gamma) = \frac{\pi}{2k_\gamma^2} \frac{2J+1}{2I+1} \frac{\Gamma_\gamma \Gamma_n}{(E_\gamma - E_\lambda - \Delta(E))^2 + \frac{\Gamma^2}{4}}, \quad (1)$$

where  $k_\gamma = E_\gamma/\hbar c$  stands for the photon wave number,  $I$  for ground state spin,  $\Gamma_\gamma$  for the ground state radiative width,  $\Gamma_n$  for the neutron decay width, the total decay width  $\Gamma = \Gamma_\gamma + \Gamma_n$ , and  $E_\lambda$  corresponds to the energy eigenvalue. The level shift  $\Delta(E)$  is given by

$$\Delta(E) = -\gamma^2 (S(E) - B), \quad (2)$$

with the reduced width  $\gamma^2$ , the shift factor  $S(E)$  and the boundary condition parameter  $B$  (see Ref. [17]).

Then for a  $1/2^+$  level in  ${}^9\text{Be}$  excited by  $E1$   $\gamma$  radiation and decaying by  $s$ -wave neutrons, and for an energy  $E = E_\gamma - S_n > 0$ , one has

$$\Gamma_\gamma = \frac{16\pi}{9} e^2 k_\gamma^3 B(E1, k)_\downarrow, \quad (3)$$

$$\Gamma_n = 2\sqrt{\epsilon(E_\gamma - S_n)}, \quad (4)$$

with  $k_\gamma = E_x/\hbar c$  being the photon momentum transfer (called photon point),  $B(E1, k)_\downarrow$  the reduced transition strength at the photon point for the decay,  $\epsilon = 2\mu a^2 \gamma^4/\hbar^2 > 0$ , where  $\mu$  and  $a$  are the reduced mass and the  ${}^8\text{Be} + n$  channel radius, respectively, and  $S_n({}^9\text{Be}) = 1.6654$  MeV [5] the neutron threshold energy. The boundary condition parameter  $B$  is taken to be zero and the shift factor  $S(E) = 0$  for  $s$ -wave neutrons [17] and thus,  $\Delta(E) = 0$ .

Since  $\Gamma_n \gg \Gamma_\gamma$ , the total resonance width  $\Gamma \approx \Gamma_n$  and the energy dependence of the photoabsorption cross section of Eq. (1) is reduced to

$$\sigma_{\gamma, n}(E_\gamma) = \frac{16\pi^2 e^2}{9 \hbar c} \frac{2J+1}{2I+1} \frac{B(E1, k)_\downarrow}{E_\gamma \sqrt{\epsilon(E_\gamma - S_n)}} \times \frac{1}{(E_\gamma - E_R)^2 + \epsilon(E_\gamma - S_n)}. \quad (5)$$

The resonance energy  $E_R$  is calculated from

$$E_R = E_\lambda + \Delta, \quad (6)$$

and the resonance width using Eq. (4)

$$\Gamma_R(E_R) = 2\sqrt{\epsilon(E_R - S_n)}. \quad (7)$$

It should be noted that because of the asymmetric line shape the resonance energy  $E_R$  does not coincide with the excitation energy at the maximum of the cross section, and the resonance width  $\Gamma_R$  differs from the FWHM.

#### B. Extraction of equivalent $(\gamma, n)$ cross sections and $B(E1)$ transition strength from the $(e, e')$ data

Equation (5) holds also for the relation between the  $(e, e')$  cross sections and the reduced transition strength if  $B(E1, k)$  is replaced by the corresponding value at finite momentum transfer  $B(E1, q)$ . (Note that in the following  $B(E1, q)_\uparrow = (2J_f + 1)/(2J_i + 1) B(E1, q)_\downarrow$  is given, where  $J_{i, f}$  denote the spins of initial and final state, respectively). If interference with transitions to higher-lying  $1/2^+$  resonances can be neglected, the equivalent  $\sigma_{\gamma, n}$  cross sections can be determined from the electron scattering results by extrapolating the reduced transition strength  $B(E1, q)$  measured at finite momentum transfer  $q$  to the photon point  $k = E_x/\hbar c$ .

Figure 2 presents the momentum transfer dependence of the measured  $(e, e')$  cross sections normalized to the Mott cross section for the transition to the first  $1/2^+$  state in  ${}^9\text{Be}$ . Besides the data from the present work displayed as squares, results of previous experiments at comparable momentum transfers shown as triangles (Ref. [12]) and circles (Ref. [7]) are included. In first-order perturbation theory inclusive electron scattering cross sections factorize in a longitudinal ( $C$ ) and a transverse ( $E$ ) part reflecting the respective polarization of the exchanged virtual photon. The kinematics of the data shown in Fig. 2 favor longitudinal excitation and thus  $B(C1, q)$  rather than  $B(E1, q)$  is determined. Both quantities can be related by Siegert's theorem  $B(E1, q) = (k/q)^2 B(C1, q)$ , i.e., they should be equal at the photon point  $q = k$ .

There are two methods to perform the extrapolation from finite momentum transfer to the photon point: (i) based on microscopic model calculations, or (ii) the plane wave Born approximation (PWBA) for a nearly model-independent extraction. The latter method is valid only

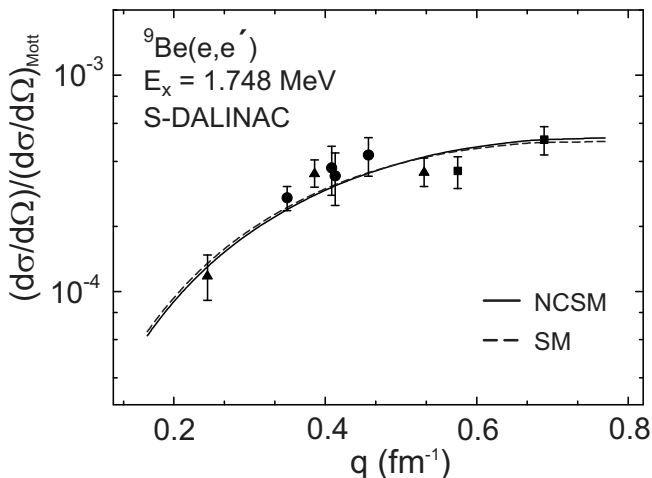


FIG. 2: Ratio of the measured cross sections to the Mott cross section of the transition to the  $1/2^+$  state in  ${}^9\text{Be}$  as a function of momentum transfer. Data are from Ref. [12] (triangles), Ref. [7] (circles) and present work (squares). Solid and dashed lines are theoretical predictions of the SM and NCSM calculations described in the text normalized to the data.

at small momentum transfers ( $q < 1 \text{ fm}^{-1}$ ) and for small atomic numbers  $Z$  ( $\alpha Z \ll 1$ ).

For an application of the first method shell-model (SM) calculations of the electroexcitation of the  $1/2^+$  state were performed with the interaction of Warburton and Brown [18] coupling  $1p$  and  $2s1d$ -shells. The formalism for calculating electron scattering form factors from the shell-model one-body transition densities is described in Ref. [19]. A similar calculation of an  $E1$  longitudinal form factor for a transition in  ${}^{12}\text{C}$  is described in Ref. [20]. Spurious states are removed with the Gloeckner-Lawson method [21]. The SM one-body transition density is dominated by the  $0p_{1/2} \rightarrow 1s_{1/2}$  neutron transition. For these two orbitals we used Hartree-Fock radial wave functions obtained with the SKX Skyrme interaction [22] with their separation energies constrained to be 1.665 MeV and 0.2 MeV, respectively. Harmonic oscillator radial wave functions were used for all other orbitals. The result normalized to the data is shown in Fig. 2 as dashed line.

Alternatively, a no-core shell model calculation (NCSM) was performed in the framework of the model described in Ref. [23] (solid line in Fig. 2). This calculation utilized the realistic nucleon-nucleon interaction CD-Bonn 2000 using very large model spaces, viz.  $8(9) \hbar\omega$  for the  $3/2^-(1/2^+)$  state, and a HO frequency of 12 MeV. Despite the large model spaces and improved convergence techniques [24], no convergence was achieved for the wave function of the  ${}^9\text{Be}$ ,  $1/2^+$  state. One should note that these calculations treat the  $1/2^+$  state in a quasibound approximation.

The two calculations predict a very similar momentum transfer dependence which describes the data well. However, the absolute magnitudes are underpredicted by

factors 3.6 (SM) and 1.7 (NCSM), respectively. Normalizing the theoretical predictions ( $B(E1, k) \uparrow = 0.008 e^2 \text{fm}^2$  (SM) and  $0.016 e^2 \text{fm}^2$  (NCSM), respectively) to the experimental data one finds  $B(E1, k) \uparrow = 0.027(2) e^2 \text{fm}^2$  using the NCSM and  $B(E1, k) \uparrow = 0.029(2) e^2 \text{fm}^2$  using the SM form factor. Both results agree with each other within error bars.

An alternative independent method to derive the  $E1$  transition strength is based on a PWBA analysis (see e.g. Ref. [25]). At low momentum transfers the form factor can be expanded in a power series of  $q$

$$\sqrt{B(E1, q)} = \sqrt{B(E1, 0)} \left( 1 - \frac{R_{tr}^2 q^2}{10} + \frac{R_{tr}^4 q^4}{280} - \dots \right), \quad (8)$$

where higher powers of  $q$  are negligible in the momentum transfer range studied in the present experiment. The so-called transition radius  $R_{tr}$  is given by  $R_{tr}^2 = \langle r^{\lambda+2} \rangle_{tr} / \langle r^\lambda \rangle_{tr}$ , where  $\langle r^\lambda \rangle_{tr}$  denotes the moments of the transition density

$$\langle r^\lambda \rangle_{tr} = 4\pi \int \rho_{tr} r^{\lambda+2} dr. \quad (9)$$

An additional assumption is made that  $R_{tr}^4$  can be parameterized in the form  $R_{tr}^4 = a(R_{tr}^2)^2$ , where the parameter  $a$  is determined using theoretical transition densities.

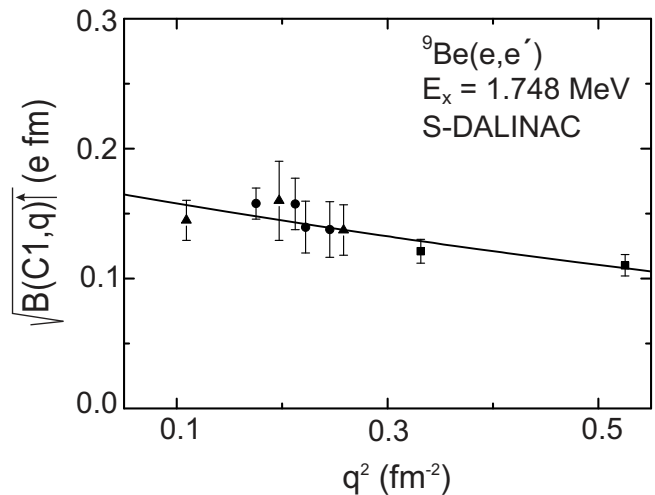


FIG. 3: Ratio of the measured cross sections of the transition to the  $1/2^+$  state in  ${}^9\text{Be}$  to the Mott cross sections as a function of the squared momentum transfer. The solid line is a fit of Eq. (8) with parameters  $\sqrt{B(C1, 0)} = 0.164(12) \text{ efm}$  and  $R_{tr} = 2.9(3) \text{ fm}$

Since the above relation (8) holds in the plane wave limit only, distorted wave Born approximation (DWBA) correction factors have been calculated based on the NCSM results in order to convert the measured cross sections into equivalent PWBA cross sections. Corrections of the order 10% are obtained. Figure 3 presents the so corrected data as a function of the squared momentum transfer. The solid line shows a fit of Eq. (8) with parameters  $\sqrt{B(C1, 0)} = 0.164(12) \text{ efm}$  and  $R_{tr} = 2.9(3) \text{ fm}$ .

Extrapolation of the transition strength to the photon point yields  $B(E1, k) \uparrow = 0.027(4) e^2 \text{fm}^2$  in agreement with the results obtained from the analysis based on microscopic form factors.

A significant difference to the corresponding  $B(E1, k) \uparrow$  strength deduced from the real-photon experiment is observed, which finds  $0.0535(35) e^2 \text{fm}^2$  (cf. Tab. I), about a factor of two larger than the present result. This implies a severe violation of Siegert's theorem. Its origin is presently unclear but possible explanations could lie in the quasibound approximation used in the shell-model calculations and/or a need to modify the  $E1$  operator. A detailed discussion of this interesting problem is postponed to a future publication.

### C. Resonance parameters

Figure 4 shows the photoneutron cross sections of the first excited state in  ${}^9\text{Be}$  extracted from the present work (top and middle) together with the previous (bottom) result of Ref. [7]. The data are summed in 15 keV bins. All three data sets are in good agreement with each other.

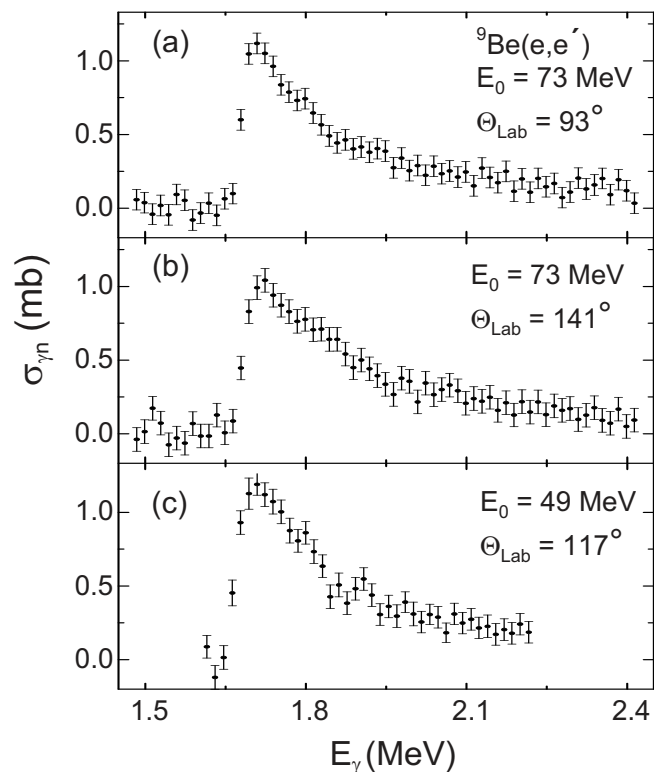


FIG. 4: Photoneutron cross sections extracted from the present (top and middle) and older (bottom)  $(e, e')$  data [7].

Since all three measurements shown in Fig. 4 were independent, the data can be averaged. The resulting averaged  $(\gamma, n)$  cross sections are presented in the upper part of Fig. 5. The solid line is a fit with Eq. (5). In or-

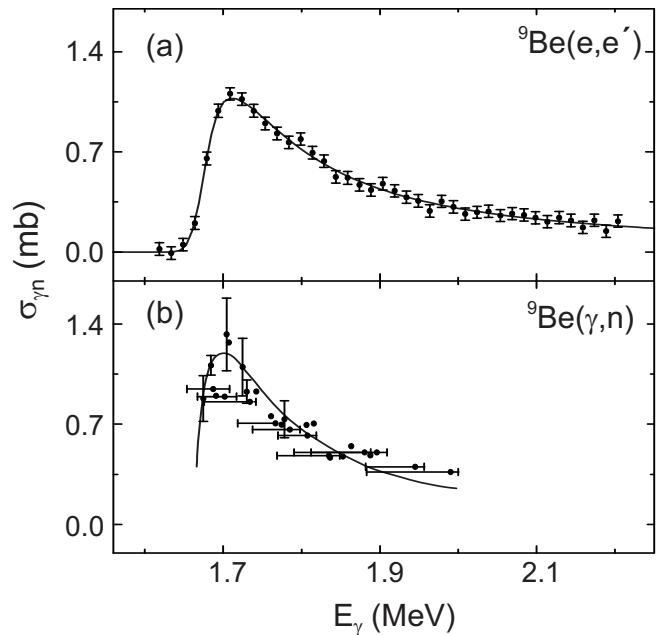


FIG. 5: Averaged photoneutron cross sections extracted from the  $(e, e')$  data shown in Fig. 4 in comparison with the cross sections extracted from the latest  ${}^9\text{Be}(\gamma, n)$  experiments [6]. The solid lines are the corresponding fits with Eq. (5) with the parameters given in the text.

der to account for the detector response the theoretical form is folded with the experimental resolution function. Since the experimental resolution was much smaller than the resonance width, the influence of the resolution function is small except for energies around the maximum of the cross sections. The fit results in a resonance energy  $E_R = 1.748(6)$  MeV and a width  $\Gamma_R = 274(8)$  keV in contradiction to the results of Ref. [7] but in agreement with the reanalysis of Barker [11]. In fact, since the data of KÜchler et al. [7] are very close to those of the present work (cf. Fig. 4) an independent reanalysis yields resonance parameters very similar to the ones from the new data. The most likely explanation for the values given in Ref. [7] is that the maximum energy and FWHM instead of the true resonance parameters were quoted. The final results are included in Tab. I.

The lower part of Fig. 5 shows the measured  ${}^9\text{Be}(\gamma, n)$  cross sections of Utsunomiya et al. [6]. Application of Eq. (5) leads to comparable resonance parameters  $E_R = 1.750(10)$  MeV and  $\Gamma_R = 283(42)$  keV but the present work provides values with considerably improved uncertainties.

## IV. ASTROPHYSICAL IMPLICATIONS

To calculate the thermonuclear reaction rate of  $\alpha(an, \gamma){}^9\text{Be}$  in a wide range of temperatures, we numerically integrate the thermal average of cross sections  $N_A^2 \langle \sigma v \rangle$  (as defined e.g. in Ref. [13]) assuming two-step

formation of  ${}^9\text{Be}$  through a metastable  ${}^8\text{Be}$ . The formation through  ${}^5\text{He}$  followed by an  $\alpha$  capture is generally neglected because of the short lifetime of  ${}^5\text{He}$  except for the work of Ref. [26] which indicates relevance of this channel at  $T \gg T_9$  (see, however, the criticism in Ref. [27]). The same formulation to the  ${}^9\text{Be}$  formation is also used in the NACRE compilation [13]. Resonant and non-resonant contributions from the  $\alpha + \alpha \rightarrow {}^8\text{Be}$  reaction are taken into account. The ground state of  ${}^8\text{Be}$  is described by a resonance energy  $E_R = 0.0918$  MeV with respect to  $\alpha + \alpha$  threshold and a width  $\Gamma_\alpha = 5.57(25)$  eV taken from Ref. [5]. Elastic cross sections of  $\alpha\alpha$  scattering were treated as described in Ref. [28].

The resonance properties (energy,  $\gamma$  and neutron decay widths) of the lowest excited states in  ${}^9\text{Be}$  with the corresponding g.s. branching ratios  $f$  included into the calculation of the  $\alpha(\alpha n, \gamma){}^9\text{Be}$  reaction rate are summarized in Tab. II. An energy dependence of the partial decay widths was taken into account only for the  $1/2^+$  resonance.

TABLE II: Low-lying states in  ${}^9\text{Be}$  considered in the calculations of the  $\alpha(\alpha n, \gamma){}^9\text{Be}$  reaction rate. The quantity  $f$  denotes the branching ratio of the corresponding state into the  $n + {}^8\text{Be}$  decay channel.

$J^\pi$	$E_R$ (MeV)	$\Gamma_\gamma$ (eV)	$\Gamma_n$ (MeV)	$f$ (%)	Ref.
$1/2^+$	1.748(6)	0.302(45)	0.274(8)	100	Present
$5/2^-$	2.4294(13)	0.089(10)	0.78(13)	7(1)	[5]
$1/2^-$	2.78(12)	0.45(36)	1.08(11)	100	[5, 13]
$5/2^+$	3.049(9)	0.90(45)	0.282(110)	87(13)	[5, 13]

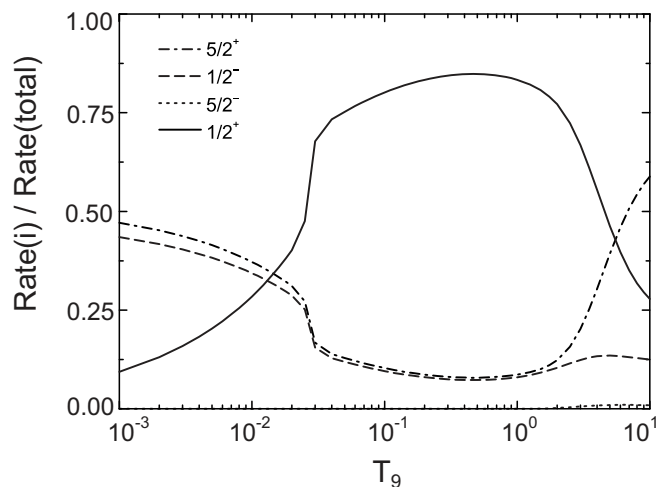


FIG. 6: Contributions of the lowest-lying states (i) in  ${}^9\text{Be}$  to the  $\alpha(\alpha n, \gamma){}^9\text{Be}$  reaction rate.

Reaction rates calculated at representative temperatures are given in Tab. III.

Figure 6 shows the individual contributions of the excited states considered in Tab. II to the total reaction

TABLE III: The thermonuclear reaction rate  $N_A^2(\sigma v)$  of  $\alpha(\alpha n, \gamma){}^9\text{Be}$  at representative temperatures.

$T_9$	Rate	$T_9$	Rate	$T_9$	Rate
0.001	$4.67 \cdot 10^{-59}$	0.04	$7.53 \cdot 10^{-16}$	0.5	$3.93 \cdot 10^{-07}$
0.002	$2.82 \cdot 10^{-47}$	0.05	$1.07 \cdot 10^{-13}$	0.6	$3.91 \cdot 10^{-07}$
0.003	$1.45 \cdot 10^{-41}$	0.06	$2.74 \cdot 10^{-12}$	0.7	$3.70 \cdot 10^{-07}$
0.004	$5.77 \cdot 10^{-38}$	0.07	$2.68 \cdot 10^{-11}$	0.8	$3.41 \cdot 10^{-07}$
0.005	$2.11 \cdot 10^{-35}$	0.08	$1.43 \cdot 10^{-10}$	0.9	$3.11 \cdot 10^{-07}$
0.006	$1.90 \cdot 10^{-33}$	0.09	$5.17 \cdot 10^{-10}$	1	$2.81 \cdot 10^{-07}$
0.007	$6.97 \cdot 10^{-32}$	0.1	$1.41 \cdot 10^{-09}$	1.25	$2.18 \cdot 10^{-07}$
0.008	$1.36 \cdot 10^{-30}$	0.11	$3.17 \cdot 10^{-09}$	1.5	$1.71 \cdot 10^{-07}$
0.009	$1.69 \cdot 10^{-29}$	0.12	$6.12 \cdot 10^{-09}$	1.75	$1.37 \cdot 10^{-07}$
0.01	$1.49 \cdot 10^{-28}$	0.13	$1.06 \cdot 10^{-08}$	2	$1.12 \cdot 10^{-07}$
0.011	$9.96 \cdot 10^{-28}$	0.14	$1.67 \cdot 10^{-08}$	2.5	$7.90 \cdot 10^{-08}$
0.012	$5.38 \cdot 10^{-27}$	0.15	$2.46 \cdot 10^{-08}$	3	$6.00 \cdot 10^{-08}$
0.013	$2.44 \cdot 10^{-26}$	0.16	$3.43 \cdot 10^{-08}$	3.5	$4.81 \cdot 10^{-08}$
0.014	$9.60 \cdot 10^{-26}$	0.18	$5.86 \cdot 10^{-08}$	4	$4.00 \cdot 10^{-08}$
0.015	$3.34 \cdot 10^{-25}$	0.2	$8.79 \cdot 10^{-08}$	5	$2.97 \cdot 10^{-08}$
0.016	$1.05 \cdot 10^{-24}$	0.25	$1.71 \cdot 10^{-07}$	6	$2.32 \cdot 10^{-08}$
0.018	$7.98 \cdot 10^{-24}$	0.3	$2.50 \cdot 10^{-07}$	7	$1.87 \cdot 10^{-08}$
0.02	$4.65 \cdot 10^{-23}$	0.35	$3.11 \cdot 10^{-07}$	8	$1.53 \cdot 10^{-08}$
0.025	$1.86 \cdot 10^{-21}$	0.4	$3.54 \cdot 10^{-07}$	9	$1.27 \cdot 10^{-08}$
0.03	$1.97 \cdot 10^{-19}$	0.45	$3.80 \cdot 10^{-07}$	10	$1.06 \cdot 10^{-08}$

rate as a function of temperature. The  $1/2^+$  state (solid line) dominates in the temperature range  $T_9 = 0.04 - 3$ . The role of the  $5/2^-$  state (dotted line) is negligible small at all temperatures. At values  $T_9 < 0.04$  the low-energy tails of the broad  $1/2^-$  (dashed line) and  $5/2^+$  (dashed-dotted line) resonances become increasingly important. Temperatures in supernova II scenarios reach values well above  $T_9$ . Under these conditions, the maximum of the photon spectrum is shifted to energies above the  $1/2^+$  state and the  $5/2^+$  state starts to dominate when approaching  $T_9 = 10$ .

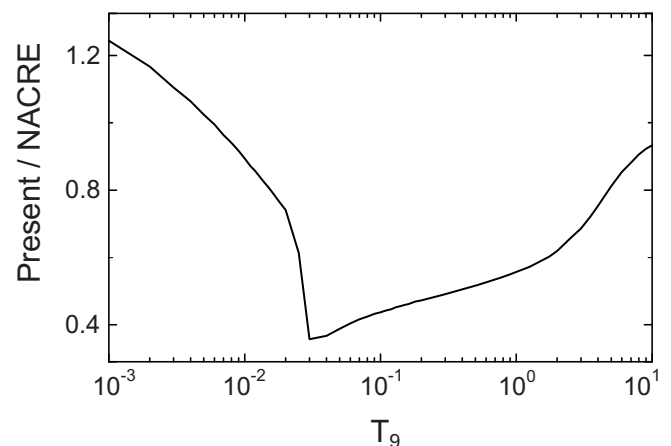


FIG. 7: The ratio of the present rate to the latest NACRE compilation [13]. Deviations ranges from +25% to -60% depending on the temperature.

The ratio of the present reaction rates to the latest

NACRE compilation [13] is shown in Fig. 7. Deviations ranges from +20% to -60% depending on the temperature. Besides using the improved resonance parameters of the  $1/2^+$  state, there are some differences between the present calculation and the one described in Ref. [13]. The  $5/2^-$  state is neglected in the latter case. However, as can be seen in Fig. 6 its contributions are very small. Also the  $^8\text{Be}$  g.s. parameters taken from [5] differ from those used in Ref. [13]. The pronounced kink at  $T_9 = 0.03$  in Fig. 7 marks the onset of resonant contributions in the  $\alpha + \alpha \rightarrow ^8\text{Be}$  cross sections. Rates from a semimicroscopic three-body model [29] are also available for temperatures  $0.2 \leq T_9 \leq 5$ . These are typically about 20% larger than the NACRE results.

The difference observed for the  $\gamma$  decay width of the  $1/2^+$  resonance between the measurements of Utsumomiya et al. [6] and the present work have a non-negligible impact on the reaction rates. In general, taking a larger  $\Gamma_\gamma$  the contribution of the  $1/2^+$  resonance will increase reducing the deviations from the NACRE result at high temperatures. It should also be noted that non-resonant contributions to the  $^8\text{Be}(n, \gamma)^9\text{Be}$  neglected in both approaches discussed above may be relevant [30]. The calculations described in Refs. [30, 31] suggest sizable effects while Ref. [26] finds it to be of minor importance. Finally, there is a recent claim [32] that the picture of a sequential formation is incorrect for the near-threshold  $1/2^+$  state and it should be described as a genuine three-body process [33]. This would modify the resonance parameters considerably.

## V. CONCLUDING REMARKS

The astrophysical relevant  $^9\text{Be}(\gamma, n)$  cross sections have been extracted from  $^9\text{Be}(e, e')$  data. The resonance parameters of the first excited  $1/2^+$  state in  $^9\text{Be}$  are derived in a one-level  $R$ -matrix approximation. The resonance parameters averaged over all available  $(e, e')$  data are  $E_R = 1.748(6)$  keV and  $\Gamma_R = 274(8)$  keV in agreement with the latest direct  $(\gamma, n)$  experiment [6] but with much improved uncertainties. However, the deduced  $\gamma$  decay width is about a factor of two smaller. Rates for the temperature-dependent formation of  $^9\text{Be}$  under stellar conditions are given. They differ significantly from the values adopted in the NACRE compilation [13]. Fur-

ther improvements of the reaction rate require the inclusion of direct capture reactions.

The difference in the  $B(E1)$  transition strength obtained from electron- and photon-induced reaction presents an intriguing problem. Since the present result is extracted from the longitudinal form factor, it might indicate a violation of Siegert's theorem at the photon point. A similar problem was observed in the electro-excitation of  $1^-$  levels in  $^{12}\text{C}$  [20],  $^{16}\text{O}$  [34, 35], and  $^{40}\text{Ca}$  [36]. There, isospin mixing was offered as an explanation leading to modified form factors of longitudinal and transverse electron scattering at small momentum transfers. Another explanation could be the need for a modification of the  $E1$  operator due to meson-exchange currents. A detailed study of the weak transverse form factor of the transition to the  $1/2^+$  resonance in  $^9\text{Be}$  would be highly desirable to clarify the origin of the discrepancy.

The shell-model calculations seem to describe the momentum transfer dependence of the electron scattering data for the measured  $q$  range but fall short of the experimental transition strength. One possible explanation may be the quasibound approximation applied in the description of the  $1/2^+$  state. Near-threshold  $\alpha$ -cluster states are expected to have an increased size which amplifies the dependence on tails of the wave function like e.g. observed for the case of the Hoyle state in  $^{12}\text{C}$  [37, 38]. Calculations with improved radial wave function would be important. Also, the role of direct three-body decay needs to be further explored.

## Acknowledgments

H.-D. Gräf and the S-DALINAC team is thanked for preparing excellent beams and M. Chernykh for his help in data taking. The experiment originated from discussion of one of us (A.R.) with the late Fred Barker on an inconsistency of the analysis of the data in Ref. [7], and we are grateful for Fred's advice. Discussions with A. S. Jensen, G. Martínez-Pinedo, A. Mengoni, and S. Typel are gratefully acknowledged. This work has been supported by the DFG under contract SFB 634, and by the NSF, grant PHY-0758099. One of us (CF) acknowledges financial support from the Swedish Research Council and the European Research Council under the FP7.

- 
- [1] S. E. Woosley and R. D. Hoffman, *Astrophys. J.* **395**, 202 (1992).
  - [2] B. S. Meyer, G. J. Mathews, W. M. Howard, S. E. Woosley, and R. D. Hoffman, *Astrophys. J.* **399**, 656 (1992).
  - [3] W. M. Howard, S. Goriely, M. Rayet, and M. Arnould, *Astrophys. J.* **417**, 713 (1993).
  - [4] S. E. Woosley, J. R. Wilson, G. J. Mathews, R. D. Hoffman, and B. S. Meyer, *Astrophys. J.* **433**, 229 (1994).
  - [5] D. R. Tilley, J. H. Kelley, J. L. Godwin, D. J. Millener, J. E. Purcell, C. G. Sheua, and H. R. Weller, *Nucl. Phys.* **A745**, 155 (2004).
  - [6] H. Utsumomiya, Y. Yonezawa, H. Akimune, T. Yamagata, M. Ohta, M. Fujishiro, H. Toyokawa, and H. Ohgaki, *Phys. Rev.* **C63**, 018801 (2000).
  - [7] G. K uchler, A. Richter, and W. von Witsch, *Z. Phys. A* **326**, 447 (1987).
  - [8] J. P. Glickman, W. Bertozzi, T. N. Butti, S. Dixit,

- F. W. Hersman, C. E. Hyde-Wright, M. V. Hynes, R. W. Lourie, and B. E. Norum, *Phys. Rev.* **C43**, 1740 (1991).
- [9] I. Mukha, M. Kavatsyuk, A. Algora, L. Batist, A. Blazhev, J. Döring, H. Grawe, M. Hellström, O. Kavatsyuk, R. Kirchner, et al., *Nucl. Phys. A* **758**, 647c (2005).
- [10] F. Barker and H. Fynbo, *Nucl. Phys. A* **776**, 52 (2006).
- [11] F. C. Barker, *Aust. J. Phys.* **53**, 247 (2000).
- [12] H.-G. Clerc, K. J. Wetzel, and E. Spamer, *Nucl. Phys. A* **120**, 441 (1968).
- [13] C. Angulo, M. Arnould, M. Rayet, P. Descouvemont, D. Baye, C. Leclercq-Willain, A. Coc, S. Barhoumi, P. Aguer, C. Rolfs, et al., *Nucl. Phys. A* **656**, 3 (1999).
- [14] T. Walcher, R. Frey, H.-D. Gräf, E. Spamer, and H. Theissen, *Nucl. Instrum. Methods* **153**, 17 (1978).
- [15] A. W. Lenhardt, U. Bonnes, O. Burda, P. von Neumann-Cosel, M. Platz, A. Richter, and S. Watzlawik, *Nucl. Instrum. Methods Phys. Res. A* **562**, 320 (2006).
- [16] F. Hofmann, P. von Neumann-Cosel, F. Neumeyer, C. Rangacharyulu, B. Reitz, A. Richter, G. Schrieder, D. I. Sober, L. W. Fagg, and B. A. Brown, *Phys. Rev. C* **65**, 024311 (2002).
- [17] A. M. Lane and R. G. Thomas, *Rev. Mod. Phys.* **30**, 257 (1958).
- [18] E. K. Warburton and B. A. Brown, *Phys. Rev. C* **46**, 923 (1992).
- [19] B. A. Brown, B. H. Wildenthal, C. F. Williamson, F. N. Rad, S. Kowalski, H. Crannell, and J. T. O'Brien, *Phys. Rev. C* **32**, 1127 (1985).
- [20] M. C. A. Campos, P. von Neumann-Cosel, F. Neumeyer, A. Richter, G. Schrieder, E. Spamer, B. A. Brown, and R. J. Peterson, *Phys. Lett. B* **349**, 433 (1995).
- [21] D. H. Gloeckner and R. D. Lawson, *Phys. Lett. B* **53**, 313 (1974).
- [22] B. A. Brown, *Phys. Rev. C* **58**, 220 (1998).
- [23] C. Forssén, P. Navrátil, W. E. Ormand, and E. Caurier, *Phys. Rev. C* **71**, 044312 (2005).
- [24] C. Forssén, J. P. Vary, E. Caurier, and P. Navrátil, *Phys. Rev. C* **77**, 024301 (2008).
- [25] H. Theissen, *Springer Tracts Mod. Phys.* **65**, 1 (1972).
- [26] L. Buchmann, E. Gete, J. C. Chow, J. D. King, and D. F. Measday, *Phys. Rev. C* **63**, 034303 (2001).
- [27] L. V. Grigorenko and M. V. Zhukov, *Phys. Rev. C* **72**, 015803 (2005).
- [28] K. Nomoto, F.-K. Thielemann, and S. Miyaji, *Astron. Astrophys.* **149**, 239 (1985).
- [29] V. D. Efros, H. Oberhummer, A. Pushkin, and I. J. Thompson, *Eur. Phys. J. A* **1**, 447 (1998).
- [30] A. Mengoni and T. Otsuka, *AIP Conf. Proc.* **529**, 119 (2000).
- [31] J. Görres, H. Herndl, I. J. Thompson, and M. Wiescher, *Phys. Rev. C* **52**, 2231 (1995).
- [32] E. Garrido, D. V. Fedorov, and A. S. Jensen, *Phys. Lett. B* **684**, 132 (2010).
- [33] R. Álvarez-Rodríguez, H. O. U. Fynbo, A. S. Jensen, and E. Garrido, *Phys. Rev. Lett.* **100**, 192501 (2008).
- [34] H. Miska, H. D. Gräf, A. Richter, D. Schüll, E. Spamer, and O. Titze, *Phys. Lett. B* **59**, 441 (1975).
- [35] J. Friedrich and N. Voegler, *Phys. Lett. B* **217**, 220 (1989).
- [36] H. D. Gräf, V. Heil, A. Richter, E. Spamer, W. Stock, and O. Titze, *Phys. Lett. B* **72**, 179 (1977).
- [37] M. Chernykh, H. Feldmeier, T. Neff, P. von Neumann-Cosel, and A. Richter, *Phys. Rev. Lett.* **98**, 032501 (2007).
- [38] M. Chernykh, H. Feldmeier, T. Neff, P. von Neumann-Cosel, and A. Richter, *Phys. Rev. Lett.* (in press).